Photoinduced Electron and Proton Transfer in Phenol and Its Clusters with Water and Ammonia†

Andrzej L. Sobolewski*,‡ and Wolfgang Domcke§

Institute of Physics, Polish Academy of Sciences, PL-02668 Warsaw, Poland, and Institute of Physical and Theoretical Chemistry, Technical University of Munich, D-85747 Garching, Germany

Received: April 4, 2001; In Final Form: May 22, 2001

Ab initio (RHF, MP2, CASSCF, and CASPT2) calculations have been performed for the electronic ground and lowest excited singlet states of phenol, the complexes of phenol with water and ammonia, and the corresponding cations. In agreement with recent experiments it is found that proton transfer is a barrierless process in the phenol−$(H_2O)_3$ and phenol−NH_3 cations, whereas no proton transfer occurs in the phenol−H_2O cation. Novel aspects of the reaction dynamics in the excited-state manifold of the neutral clusters are revealed by the calculations. Predissociation of the $S_1(\pi\pi^*)$ state by a low-lying $^1\pi\sigma^*$ state leads to a concerted electron and proton-transfer reaction from the chromophore to the solvent. The excited-state reaction is endothermic in phenol−H_2O and phenol−$(H_2O)_3$ clusters but exothermic (though activated) in the phenol−NH_3 complex. These results substantiate recent reinterpretations of spectroscopic and kinetic data on hydrogen-transfer reactions in phenol−ammonia clusters. The close relationship of the concerted electron−proton-transfer process in phenol−water complexes with the formation of hydrated electrons in the photolysis of phenol and tyrosine in liquid water is pointed out.

1. Introduction

Phenol is the chromophore of the amino acid tyrosine. Proton- and electron-transfer processes involving amino acids play an important role in photobiology.[1] Tyrosine, in particular, plays a prominent role in the catalysis of the water-splitting reaction in photosystem II of the higher plants.[2] An essential step in the light-induced oxidation of water is the oxidation of tyrosine by electron transfer to the chlorophyll pair. In a subsequent step, a hydrogen atom from a water molecule coordinated to a manganese cluster is transferred to the tyrosine radical.[2]

Phenol−water clusters are good models for the investigation of the photoinduced elementary processes occurring in living matter. Intracluster proton-transfer (PT) processes in phenol−water (PhW) complexes have extensively been studied in recent years; see refs 3−5 for reviews. Phenol−ammonia (PhA) clusters also have served as easily accessible and versatile models of intracluster PT dynamics.[3−7] The detection schemes for the PT have been either time-resolved photoelectron spectroscopy, mass spectrometry, or IR or optical spectroscopy of educts and products.[4,6,7] Vibronic spectra of PhA_n clusters could be recorded by using the $(NH_3)_nH^+$ product yield as signal.[8] It has been a matter of debate whether the proton/hydrogen transfer occurs in the S_1 excited state or in the cluster cation or in both.[4,6,7] It has been inferred by several authors that intracluster proton transfer occurs more readily in PhA_n clusters than in PhW_n clusters. For example, proton transfer has been found to take place readily in the PhA_1 cation, while at least three water molecules are necessary for PT to occur in PhW cluster cations.[4,9]

The interpretation of the spectroscopic data on PhW_n and PhA_n clusters and cluster cations has been greatly facilitated by ab initio electronic-structure calculations. Most of the calculations have been concerned with the electronic and geometric structures of the electronic ground state of the neutral clusters[10−17] or the cluster cations.[17−20] Calculated vibrational frequencies and IR spectra also have been reported.[11,12,17,19] Less computational work has been performed for the excited states of PhW_n and PhA_n clusters. This fact reflects the significant difficulties which are generally encountered for open-shell systems. A potential-energy (PE) function for PT in the $S_1(\pi\pi^*)$ state at the CIS level has been obtained by Yi and Scheiner[15] for the PhA_1 cluster and by Siebrand et al.[21] for the PhA_5 cluster. Energies, geometries, and vibrations of the $S_1(\pi\pi^*)$ state of PhW_1 and PhW_2 clusters have been characterized by Fang with the CIS and CASSCF methods.[22,23]

The present work focuses on minimum-energy reaction paths for intracluster proton/hydrogen transfer and the corresponding energy profiles for low-lying excited states of PhW and PhA clusters and the ground states of the cluster cations. Such PE profiles have been reported by Yi and Scheiner[15] for PhA_1^+ (UHF and UMP2 levels) and the S_1 state of PhA_1 (CIS level), as well as by Siebrand et al. for the S_1 state of the PhA_5 cluster (CIS level).[21] Calculations of PE profiles for excited-state intramolecular proton transfer in systems such as malonaldehyde and salicylic acid have revealed that the simple CIS method may be unreliable for the prediction of excited-state PT barriers.[24,25] It therefore appears desirable to apply more sophisticated ab initio methods for the investigation of excited-state intracluster hydrogen-/proton-transfer reactions in PhW and PhA clusters. In the present work we report excited-state reaction paths optimized at the CASSCF level[26] and energy profiles calculated with the CASPT2 method[27] for PhW_1, PhW_3, and PhA_1 clusters. As a byproduct of these studies, we also have

† This paper was originally submitted for the Edward W. Schlag Festschrift (*J. Phys. Chem. A* **2001**, No. 23, June 14).

* Corresponding author. Fax: +48-22-8430926. E-mail: sobola@ifpan.edu.pl.

‡ Polish Academy of Sciences.

§ Technical University of Munich.

10.1021/jp011260l CCC: $20.00
Published on Web 09/15/2001

obtained PE functions for proton transfer in the corresponding cluster cations.

We stress that it has not been the goal of the present work to perform highly accurate calculations of geometric structures of reactants and products and reaction enthalpies. We have rather been interested in the development of a clear qualitative picture of the basic mechanisms of the hydrogen-/proton-transfer processes in PW and PA clusters. In addition to the calculation of PE functions, we have therefore also analyzed the electronic wave functions in terms of configurations, molecular orbitals, and charge distributions. A result of general significance is the finding that excited-state hydrogen transfer in PhW_n and PhA_n clusters is an electronically nonadiabatic process, involving the switch of the electronic configuration from the optically prepared $^1\pi\pi^*$ state to a $^1\pi\sigma^*$ state. The antibonding character of the σ^* orbital provides the driving force for the concerted electron and proton-transfer process in the $^1\pi\sigma^*$ state.

2. Computational Methods

The geometry of the systems in electronic configurations pertaining to this work was optimized using the complete-active-space self-consistent-field (CASSCF) method. Additionally, the ground-state geometry optimized with the restricted Hartree−Fock (RHF) second-order Møller−Plesset (MP2) method was used as the reference for the excited-state energy calculations. A nonstandard basis set was used. The 6-31G* split-valence double-ζ Gaussian basis set was augmented with diffuse functions for the heteroatoms and polarization functions for the hydrogen atoms involved in hydrogen bonds (6-31+G**).[28] For the $^1\pi\sigma^*$ excited-state optimizations this basis set was supplemented with a set of s and p diffuse Gaussian functions of exponent $\eta = 0.02$, localized at a floating center in order to provide additional flexibility for the description of the diffuse σ^* orbital. The position of the floating center was optimized in the course of geometry optimization. The effect of the inclusion of the floating center on the energy and geometry of the S_0 and $\pi\pi^*$ electronic states studied in this work was negligibly small. Therefore the floating center was omitted in geometry optimizations of these states.

The active space for the CASSCF geometry optimizations of the $\pi\pi^*$ excited singlet state and the ground state of the cation ($^2\pi$) includes six π valence orbitals of phenol. In the CASSCF calculations of the $\pi\sigma^*$ excited singlet state the highest π^* orbital was replaced by the σ^* orbital. In all excited-state optimizations the active space thus correlates 6 electrons in 6 orbitals.

It is nowadays well established that phenol and its clusters with single water and ammonia molecules (PhW_1 and PhA_1, respectively) are of C_s symmetry in the ground state.[10−14] C_s symmetry of the systems was thus imposed in the course of the geometry optimization. Within the C_s point group the wave function of the $^1\pi\sigma^*$ state transforms according to the A″ representation and thus cannot collapse to the ground state or to the $^1\pi\pi^*$ excited state (both states are of A′ symmetry). For technical reasons, the same restriction of symmetry was imposed during geometry optimization of the PW_3 cluster. In this case the imposition of C_s symmetry is a genuine restriction, since existing theoretical and experimental data suggest a lower symmetry configuration as the minimum of the ground state.[5,11,14] Thus, this case is to be considered only as a qualitative illustration of the effect of solvation on the photophysics of this system.

For the construction of the reaction path for hydrogen detachment from phenol and for hydrogen/proton transfer in its clusters with water and ammonia, the coordinate-driven minimum-energy-path approach was adopted. In phenol, for a given value of the OH bond length, all remaining intramolecular coordinates were optimized. For hydrogen/proton transfer from phenol to water along a preexisting hydrogen bond in phenol−water clusters, the reaction coordinate was defined as the difference of the distance between phenol oxygen and hydrogen atom ($O_{Ph}H$) and the distance between the hydrogen atom and oxygen atom of water (O_WH). In the case of the phenol−ammonia cluster, the second distance was replaced by the NH bond length formed between the hydrogen atom of phenol and the nitrogen atom of ammonia. For a given value of this reaction coordinate, all the remaining intramolecular and intermolecular degrees of freedom were optimized under the restriction of C_s symmetry.

The geometry optimizations were performed with the GAMESS package.[29] To incorporate electron-correlation effects, single-point calculations at optimized geometries were performed with the CASPT2 method (second-order perturbation theory based on the CASSCF reference).[27] The CASPT2 calculations were performed with the MOLCAS-4 package,[30] using the ANO-L basis set of split-valence double-ζ quality with polarization functions on heavy atoms and diffuse s and p Gaussian functions of exponent $\eta = 0.02$ localized at the floating center. Since the floating center position was only determined in optimizations of the $^1\pi\sigma^*$ state, in the CASPT2 calculations performed at the geometries optimized in other electronic states the diffuse Gaussian functions were localized at the center of mass of the phenol ring. In the CASPT2 calculations on phenol the active space was enlarged to include all valence π orbitals of phenol in addition to the σ^* orbital. The active space thus correlates 8 electrons in 8 orbitals. In the CASPT2 calculations on clusters of phenol with water and with ammonia, an additional π orbital, mostly localized on the oxygen atom of water or on the nitrogen atom of ammonia, respectively, was included in the active space. The same active space and basis set were used for the excited-state and for the ground-state calculations of a given system.

The results have not been corrected for the basis-set superposition error (BSSE). The BSSE has repeatedly been investigated for phenol−water clusters and related systems[5,11,31] and is typically of the order of 1 kcal/mol for the dissociation energy with basis sets of the type used here. This correction is not relevant for the present purposes.

3. Results and Discussion

A. Phenol. The ground-state equilibrium structure of phenol has been determined by several authors at various levels of theory[11,21] and need not be discussed here. The vertical excitation energy of the $S_1(\pi\pi^*)$ state has been calculated by Krauss et al.[32] with the FOCI method and by Gao et al.[33] with the CASPT2 method. The vertical excitation energies of a number of valence and Rydberg singlet states have been obtained by Lorentzon et al. with CASPT2.[34] Fang[22] has obtained the adiabatic excitation energy of the $S_1(\pi\pi^*)$ state of phenol at the CIS and CASSCF levels.

Vertical and adiabatic excitation energies and ionization potentials of the systems in electronic states considered in the present work are collected in Table 1. The energy of vertical excitation was calculated at the MP2-optimized geometry of the ground state, whereas the adiabatic excitation energy was calculated at the CASSCF-optimized geometry of a given state with respect to the ground-state energy calculated at the MP2-optimized geometry.

The calculated energy of vertical excitation to the lowest $^1\pi\pi^*$ state of phenol (4.46 eV) is similar to the energy obtained by

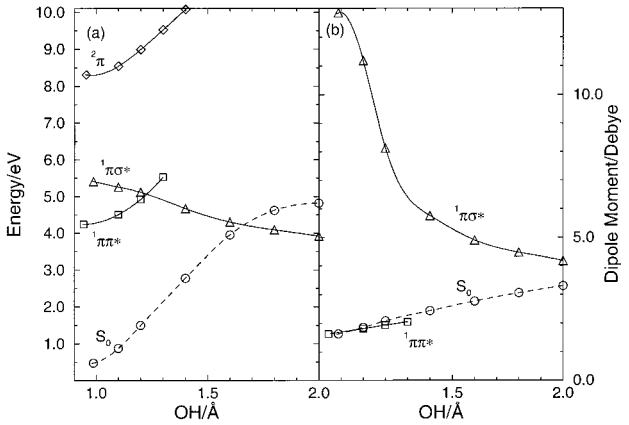

Figure 1. CASPT2 PE profiles (a) and CASSCF dipole moments (b) of phenol in the electronic ground state (circles), the lowest $^1\pi\pi^*$ excited state (squares), the lowest $^1\pi\sigma^*$ state (triangles), and the $^2\pi$ ground state of the cation (diamonds) as a function of the OH stretching coordinate.

TABLE 1: CASPT2 Vertical and Adiabatic (in Parentheses) Energies of the Lowest Excited Singlet States of the Neutral Systems and the Ground State of the Cations Studied in This Work

system	state		
	$^1\pi\pi^*$	$^1\pi\sigma^*$	$^2\pi$
phenol	4.46 (4.24)	5.77	8.46 (8.35)
phenol−H_2O	4.35 (4.17)	5.52 (4.94)	8.19 (7.80)
phenol−$(H_2O)_3$	4.23 (4.14)	5.76 (4.65)	8.02 (7.55)
phenol−NH_3	4.31 (4.20)	5.47 (4.16)	7.65 (7.49)

other authors at the same level of theory.[33,34] The calculated adiabatic excitation energy of this state without zero-point energy correction is about 0.26 eV lower than the experimental value of 36346.7 cm^{-1} (4.50 eV).[5] As usual for $^1\pi\pi^*$ states, CASPT2 tends to overestimate the dynamical electron correlation correction by a few tenths of an electronvolt, leading to an underestimation of the excitation energy. The energy of vertical excitation to the lowest $^1\pi\sigma^*$ state (5.77 eV) is similar to the value of 5.78 eV obtained by Lorentzon et al.[34] The vertical ionization energy (8.46 eV) is higher than the 8.21 eV calculated in ref 34.

In Figure 1a the CASPT2 PE profiles calculated along the minimum-energy path for detachment of the hydrogen atom of the OH group of phenol are presented. For clarity, only the lowest $^1\pi\pi^*$ and $^1\pi\sigma^*$ states and the electronic ground state of the neutral system and the ground state ($^2\pi$) of the cation are shown. The geometries of the excited states have been optimized along the reaction path, while the ground-state energy is computed at the $^1\pi\sigma^*$-optimized geometries. Inspecting the results presented in Figure 1a, one sees that the PE profiles of the ground state and the lowest valence $^1\pi\pi^*$ excited state of the neutral system as well as the ground state of cation ($^2\pi$) rise with increasing OH distance in an approximately parallel manner, while the PE profile of the $^1\pi\sigma^*$ state is essentially repulsive. The geometry-optimized $^1\pi\pi^*$ state lies below the optimized $^1\pi\sigma^*$ state and thus is the lowest excited singlet state of the system at the ground-state equilibrium geometry. It is seen from Figure 1a that the repulsive $^1\pi\sigma^*$ state predissociates the $^1\pi\pi^*$ state above a certain excess energy in the latter state.

In a multidimensional picture, the $^1\pi\pi^*-{}^1\pi\sigma^*$ curve crossing in Figure 1a develops into a conical intersection. Out-of-plane vibrational modes of A″ symmetry can lift the accidental degeneracy at the crossing point, generating a multidimensional conical intersection. The resulting lower adiabatic PE sheet of the coupled $^1\pi\pi^*-{}^1\pi\sigma^*$ states will exhibit a barrier in the vicinity of the conical intersection. A wave packet prepared in the $^1\pi\pi^*$ state by optical excitation with sufficient excess energy will bypass the conical intersection via this barrier and then evolve on the $^1\pi\sigma^*$ surface.

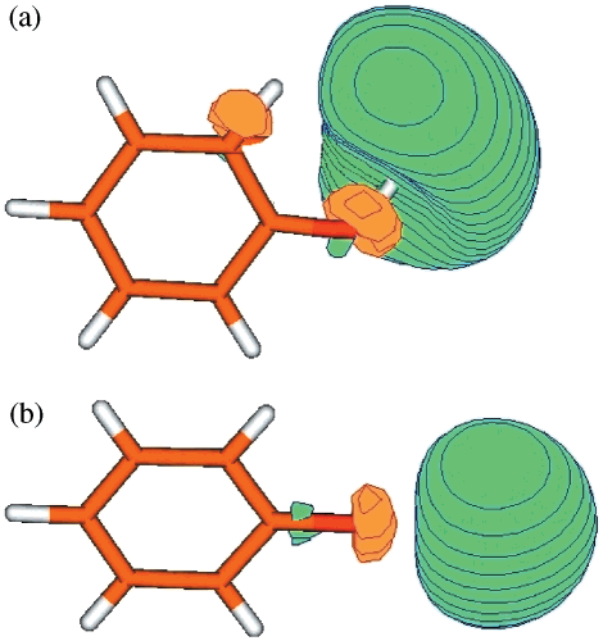

Figure 2. The σ^* orbital obtained by a CASSCF calculation for the $^1\pi\sigma^*$ state of phenol at $R_{OH} = 1$ Å (a) and $R_{OH} = 2$ Å (b).

It is seen in Figure 1a that the repulsive $^1\pi\sigma^*$ PE profile intersects the PE function of the ground state at an OH distance of about 1.65 Å, resulting in another conical intersection. In the isolated molecule, this conical intersection is expected to lead to ultrafast (femtosecond) internal conversion to the ground state. The low-energy part of the $^1\pi\pi^*$ surface is separated from the region of strong nonadiabatic interactions with the ground state by the above-mentioned barrier on the PE surface of the lowest excited singlet state. Fluorescence quenching is expected when the excess energy in the $S_1(\pi\pi^*)$ state lies above the barrier associated with the $^1\pi\pi^*-{}^1\pi\sigma^*$ conical intersection.

In Figure 1b, the dipole-moment functions of the three states S_0, $^1\pi\pi^*$, and $^1\pi\sigma^*$ of neutral phenol are displayed. The dipole moments of the excited states have been determined at the CASSCF level along the minimum-energy path for hydrogen detachment in given electronic state, while the dipole moment of the ground state was determined at the $^1\pi\sigma^*$-optimized geometry. It is seen that phenol in the ground state and in the $^1\pi\pi^*$ state is weakly polar. The dipole moments of these states depend weakly on the OH distance. The $^1\pi\sigma^*$ state, on the other hand, is highly polar at the equilibrium geometry of the electronic ground state. Its dipole moment decreases abruptly with increasing OH distance, reflecting backflow of charge from the negatively charged H atom to the aromatic ring during dissociation. Thus in all the states under consideration, phenol dissociates into neutral products, the phenoxy radical and the hydrogen atom. Only the $^1\pi\sigma^*$ state correlates to the lowest dissociation limit.

An explicit visualization of the mechanism which provides the driving force for hydrogen atom detachment in the $^1\pi\sigma^*$ state is illustrated in Figure 2. In Figure 2a we present the σ^* orbital obtained by a CASSCF calculation for the $^1\pi\sigma^*$ state at $R_{OH} = 1.0$ Å (a geometry close to the minimum of the ground state). In Figure 2b the σ^* orbital calculated at $R_{OH} = 2.0$ Å is shown for comparison. Figure 2a shows that the σ^* orbital is

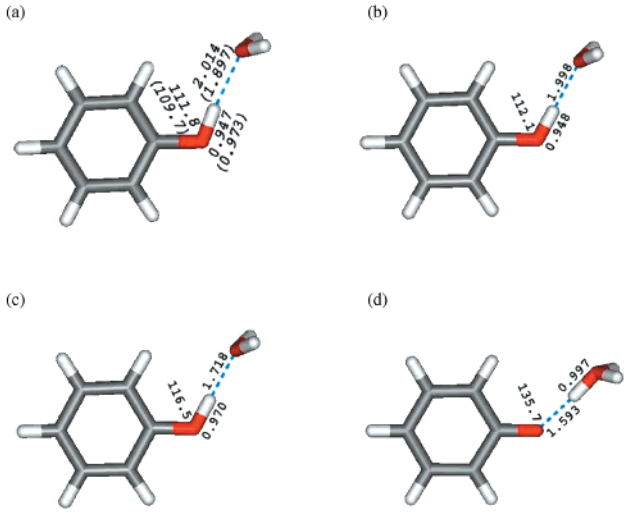

Figure 3. CASSCF equilibrium geometries of the phenol−water complex in the S_0 state (a), the $^1\pi\pi^*$ excited state (b), the $^2\pi$ state of the cation (c), and the $^1\pi\sigma^*$ excited state (d). The S_0 geometry parameters optimized at the MP2 level are indicated in parentheses.

diffuse and is largely localized near the proton of the hydroxy group. Its antibonding character with respect to the OH bond is clearly visible. Upon detachment of the proton, the σ^* orbital contracts and evolves to the 1s orbital of hydrogen (Figure 2b).

B. Phenol−H_2O. The equilibrium structure of the phenol−H_2O (PhW_1) complex optimized in the electronic ground state is shown in Figure 3a. The ground-state structure of the PhW_1 complex has been discussed in detail previously.[10,11,19,22] The complex is bound by a fairly strong hydrogen bond. We obtain an O_wH bond length of 1.897 Å at the MP2 level, longer than the 1.854 Å obtained in ref 19 but shorter than the 1.973 Å reported by Fang (both at the MP2 level).[22] The latter value is closer to our bond length obtained at the CASSCF level (2.014 Å). The structures optimized at the CASSCF level for the $^1\pi\pi^*$ state and the $^2\pi$ state of the cation are shown in Figure 3b,c, respectively. They have previously been determined and discussed.[18−20,22] As expected, the O_wH bond length slightly contracts after excitation to the $^1\pi\pi^*$ state (compare numbers presented in Figure 3a,b obtained at the CASSCF level) and is much shorter in the cation than in the neutral system, thus indicating an increase of the strength of the hydrogen bond due to excitation of an electron from the π orbital. The equilibrium geometry of the $^1\pi\sigma^*$ state shown in Figure 3d is a new result. It is seen that a hydrogen-transfer reaction has occurred: the structure represents a hydrogen-bonded complex of the phenoxy radical with the H_3O radical. The hydrogen bond connecting the two radicals is quite strong, as reflected by the rather short bond length $O_{Ph}H$ = 1.593 Å. As will become clear in a moment, the $^1\pi\sigma^*$ minimum corresponds to a hydrogen-transfer configuration rather than a proton-transfer configuration.

The CASPT2 vertical and adiabatic excitation energies of the $^1\pi\pi^*$ and of the $^1\pi\sigma^*$ states of the PhW_1 complex and the respective ionization potentials are given in Table 1. The present result of 4.17 eV for the adiabatic excitation energy of the $^1\pi\pi^*$ state implies a red shift of the S_1 state by about 0.07 eV due to complexation with water. This is in good agreement with the experimental observation (0.06 eV).[35]

In Figure 4a the CASPT2 PE profiles calculated along the minimum-energy path for the hydrogen atom transfer between phenol and water are presented. Only the lowest $^1\pi\pi^*$ and $^1\pi\sigma^*$ states and the electronic ground state of neutral system and the ground-state ($^2\pi$) of cation are considered. Similarly to the bare

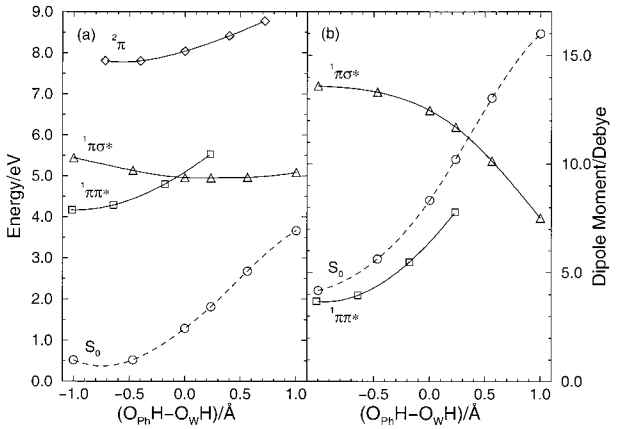

Figure 4. CASPT2 PE profiles (a) and CASSCF dipole moments (b) of the phenol−H_2O complex in the electronic ground state (circles), the lowest $^1\pi\pi^*$ excited state (squares), the lowest $^1\pi\sigma^*$ state (triangles), and the $^2\pi$ ground state of the cation (diamonds) as a function of the hydrogen-transfer reaction coordinate.

phenol case, geometries of the excited states have been optimized along the reaction path, while the ground-state energy is computed at the $^1\pi\sigma^*$-optimized geometries. The reaction coordinate is defined as the difference of the $O_{Ph}H$ and O_WH bond lengths and describes the position of the hydrogen atom relative to the oxygen atoms of phenol and water, respectively. It is seen that the PE profiles of the ground state and the lowest valence $^1\pi\pi^*$ excited state of the neutral system as well as the ground state of cation ($^2\pi$) rise with increasing reaction coordinate, although weaker than in bare phenol.

The most significant effect of complexation of phenol with a single water molecule is the removal of the conical intersection of the $^1\pi\sigma^*$ state with the S_0 state. In comparison with Figure 1a, the $^1\pi\sigma^*$ energy is pushed upward, whereas the S_0 energy increases significantly less than in bare phenol for large $O_{Ph}H$ distances. As a result, a new shallow minimum develops in the $^1\pi\sigma^*$ state at about $R_{PT} \approx 0.5$ Å (close to the CASSCF minimum with $O_{Ph}H = 1.593$ Å and $O_WH = 0.997$ Å) and the intersection with the ground state is removed. At the minimum, the hydrogen atom of phenol is transferred to the water molecule (cf. Figure 3d).

The ultrafast internal-conversion channel which exists in bare phenol when the system has reached the $^1\pi\sigma^*$ state is thus eliminated in the PhW_1 complex. In view of the relatively large $^1\pi\sigma^*-S_0$ energy gap at the minimum of the $^1\pi\sigma^*$ surface (cf. Figure 4a) and the absence of a transition dipole moment of the $^1\pi\sigma^*$ state with the ground state, the hydrogen-transferred species is presumably rather long-lived. The estimated minimum of the $^1\pi\sigma^*$ state at the CASPT2 level lies about 0.77 eV above the minimum of the $^1\pi\pi^*$ state. Thus some excess of energy in the S_1 state is needed to promote the hydrogen-transfer reaction in the PhW_1 complex.

Insight into the character of the electronic wave functions is provided by the dipole-moment functions shown in Figure 4b. Like bare phenol, the PhW_1 complex is weakly polar in the ground and in the lowest excited singlet state close to the minimum ($\mu \approx 2$ D) but is highly polar in the $^1\pi\sigma^*$ state (μ = 13.5 D) at this geometry. Unlike in phenol, the dipole moments in the S_0 and $^1\pi\pi^*$ states of the PhW_1 system increase strongly along the reaction coordinate. The rise of the dipole moment functions in the ground and in the $^1\pi\pi^*$ excited state indicates the onset of a proton-transfer reaction leading to the formation of the phenoxy radical anion and the hydronium radical cation (H_3O^+). The decrease of the dipole moment function of the $^1\pi\sigma^*$

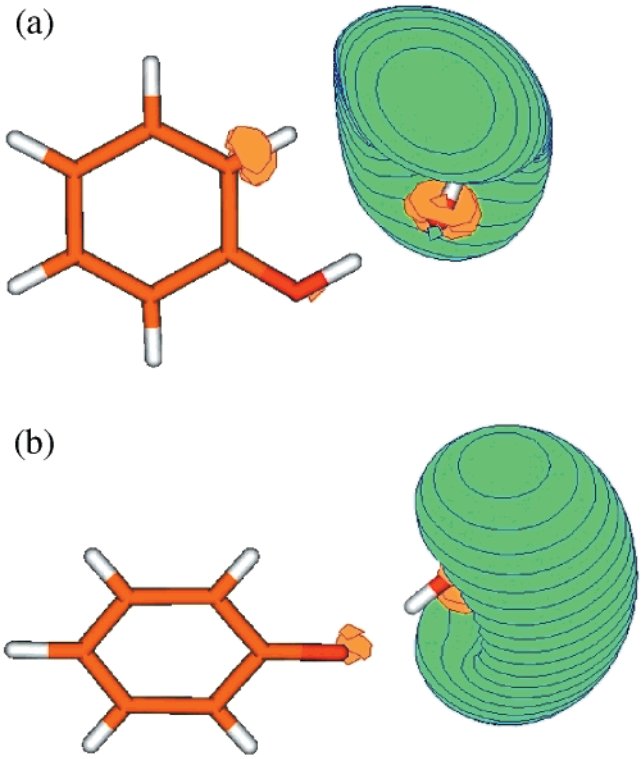

Figure 5. σ^* orbital obtained by a CASSCF calculation for the $^1\pi\sigma^*$ state of the phenol$-H_2O$ complex at the ground-state (a) and at the $^1\pi\sigma^*$-state (b) minimum geometries.

state vs the reaction coordinate is less pronounced than in the bare phenol case. The value of about 10 D calculated at the minimum of the $^1\pi\sigma^*$ state indicates a relatively high polarity of the system.

A qualitative understanding of the basic mechanism leading to a stable hydrogen-transferred structure in the $^1\pi\sigma^*$ state can be obtained from the inspection of the σ^* orbital shown in Figure 5. It is clearly seen that the σ^* orbital attaches to the water molecule already at the geometry of vertical excitation (Figure 5a). Excitation of the $^1\pi\sigma^*$ state thus involves a chromophore-to-solvent electron-transfer (ET) process.

When the geometry of the complex relaxes to the $^1\pi\sigma^*$ minimum (Figure 5b), the proton follows the electron, thus forming the phenoxy radical and the hydronium radical. They are connected by a strong hydrogen bond. It is clearly seen from Figure 5b that the hydronium radical consists of a 3s-type Rydberg orbital attached to the H_3O^+ cation. The relatively high dipole moment of the system at this nuclear configuration is the result of the high polarity of the H_3O radical: the σ^* electron cloud is displaced from the H_3O^+ cation (Figure 5b). The hydrogen-transfer reaction in the $^1\pi\sigma^*$ state is thus promoted by the electron transfer from phenol to the space surrounding the water molecule, a process which exists already at nuclear configurations close to the minima of the ground state and the $^1\pi\pi^*$ excited state (Figure 5a).

The PE function of the $^2\pi$ state of the PW_1 cluster in Figure 4a indicates that no PT takes place in PW_1^+, in agreement with previous calculations[9,11,19,20] and experiment.[4,9]

C. Phenol$-(H_2O)_3$. Detailed information on the size dependence of intracluster PT processes in small PhW_n clusters has been obtained by ingenious experimental techniques.[4,17,36,37] It has been shown that $n = 3$ is the critical size for the occurrence of PT in PhW cluster cations.[4,9] The smallest neutral cluster for which signatures of an excited-state PT have been observed

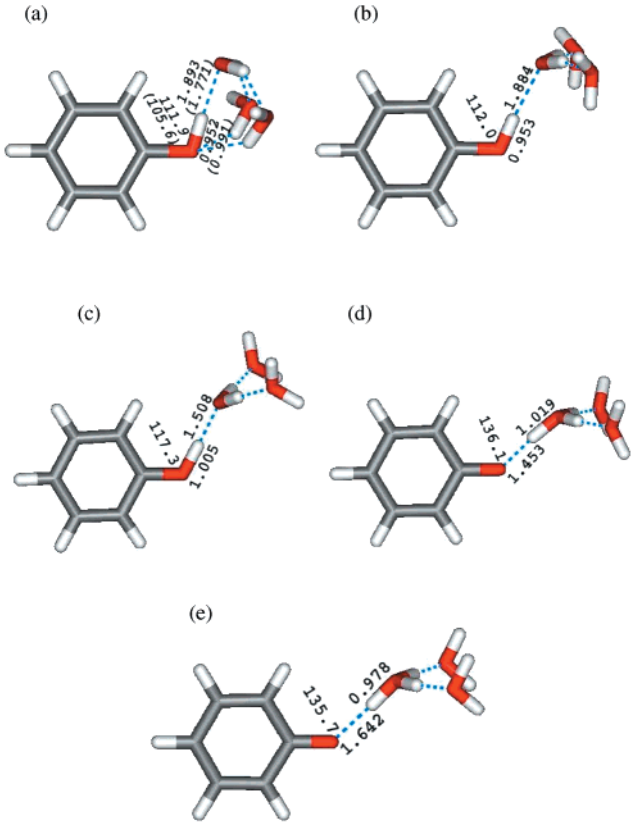

Figure 6. CASSCF equilibrium geometries of the phenol$-(H_2O)_3$ complex in the S_0 state (a) and the $^1\pi\pi^*$ excited state (b). The structures have been constrained to be of C_s symmetry. The non-PT and PT structures of the PhW_3 cation are shown in (c) and (d). The equilibrium structure of PhW_3 in the $^1\pi\sigma^*$ excited state is shown in (e). The S_0 geometry parameters optimized at the MP2 level are indicated in parentheses.

is PhW_4.[4,36,37] It has not yet been established whether a hydrogen atom transfer or ion-pair formation takes place in PhW_4*.

To obtain some information on the cluster size dependence of electron and proton-transfer processes in PhW_n clusters, we have investigated the PhW_3 complex. PhW_3 is the smallest complex beyond $n = 1$ which can possess a low-energy structure of C_s symmetry. As mentioned above, the C_s symmetry constraint is a necessity for excited-state geometry optimizations. Although the C_s contrained geometry of PhW_3 does not represent the global minimum of the S_0 and S_1 PE surfaces,[5] the energy gain by relaxation to structures of lower symmetry is of the order of a few kcal/mol.[11,38] This energy difference between different isomers in the S_0 state is of the same order of magnitude as the stabilization energy (that is, the difference between vertical and adiabatic excitation energies) of the S_1-($\pi\pi^*$) state and much smaller than the stabilization energy of the $^1\pi\sigma^*$ state, which is of the order of 1 eV (see below). The excited-state dynamics of the cluster is thus not significantly dependent on the initial geometry. Therefore, the present results on excited-state energy surfaces obtained for C_s-constrained cluster geometries can provide qualitative insight, even though the global minimum of the S_0 energy surface of the PhW_3 cluster does not possess C_s symmetry.

The geometry of the PhW_3 complex optimized in the electronic ground state with C_s symmetry constraint is shown in Figure 6a. As expected, the three water molecules from a hydrogen bond network with the OH group of phenol. We stress once more that the structure shown in Figure 6a is not the lowest energy structure of the PhW_3 cluster. The latter possesses a

cyclic water network and is of lower symmetry.[5,11,14] The structure shown in Figure 6a represents, however, a true local minimum of the S_0 surface. It serves as a reference geometry for the ensuing discussion of excited-state and PT structures.

The geometry of PhW_3 in the $^1\pi\pi^*$ state is shown in Figure 6b. The hydrogen bond between the OH group of phenol and the neighboring water is of similar strength as in the S_0 state, and the hydrogen bonds connecting the outer two water molecules with the oxygen of phenol have been broken.

For the PhW_3 cation two minima of the $^2\pi$ PE surface have been located at the CASSCF level. The corresponding structures are shown in Figure 6c,d. The structure of Figure 6c represents a phenol cation which is hydrogen bonded to a water trimer. The structure of Figure 6d, on the other hand, represents a proton-transferred configuration, in which a phenoxy radical and two water molecules are bonded to a H_3O^+ ion in the center of the complex. The proton-transferred structure of Figure 6d has previously been identified by Re and Osamura et al. at the UHF, UMP2, and DFT(B3LYP) levels[20] and Kleinermanns et al. at the ROHF level.[9]

The geometry of the PhW_3 complex optimized in the $^1\pi\sigma^*$ state is shown in Figure 6e. This structure is clearly of the hydrogen-transferred form; i.e., the hydrogen of the phenolic OH group has attached to the neighboring water molecule, forming the hydronium radical, to which the remaining two waters are hydrogen bonded. The bond lengths are $O_{Ph}H = 1.642$ Å and $O_wH = 0.978$ Å. When compared with the corresponding PW_1 complex, the transferred hydrogen atom of PW_3 is more tightly bound to the water molecule, while the hydrogen bond between the phenoxy radical and the hydronium radical is weaker than in PW_1 ($O_{Ph}H = 1.593$ Å for PW_1).

The vertical and adiabatic excitation energies of the $^1\pi\pi^*$ and $^1\pi\sigma^*$ states of PhW_3 and the adiabatic ionization potential are given in Table 1. The adiabatic energy of the latter state refers to the proton-transferred structure (Figure 6e). The results in Table 1 indicate a rather weak redshift of the adiabatic excitation energy of the $^1\pi\pi^*$ state upon complexation with water, while the adiabatic $^1\pi\sigma^*$ energy is lowered more significantly. As a result, the minimum of the $^1\pi\sigma^*$ surface, corresponding to a proton-plus-electron transferred structure, is now located only 0.51 eV above the $^1\pi\pi^*$ minimum, compared to 0.77 eV for the PhW_1 cluster (see Table 1). This is a clear indication that the $^1\pi\sigma^*$ minimum is systematically lowered relative to the $^1\pi\pi^*$ minimum with increasing size of the cluster. Also noteworthy is the very pronounced lowering of the adiabatic ionization potential with increasing number of water molecules.

The CASPT2 PE functions of the electronic states relevant for proton and hydrogen transfer in PhW_3 and PhW_3^+ are shown in Figure 7a. Comparison with the corresponding PE functions of the PhW_1 complex reveals that the minima of both the $^1\pi\pi^*$ and $^1\pi\sigma^*$ states have shifted toward larger $O_{Ph}H$ bond lengths. The $^1\pi\sigma^*$ PE function is slightly lowered with respect to the $^1\pi\pi^*$ PE function. One should have in mind that the CASPT2 approximation generally underestimates the energy of multireference states, such as the $^1\pi\pi^*$ state, relative to states dominated by a single reference, like the $^1\pi\sigma^*$ state. We can nevertheless conclude that excited-state hydrogen transfer is still endothermic in the PW_3 complex, which agrees with the experimental findings.[4,36,37] Experimentally, a hydrogen- or proton-transfer process has been identified in one of the PhW_4 clusters.[4,36,37] Further calculations of reaction-path PE functions for larger PhW_n clusters are necessary for the verification of this conclusion.

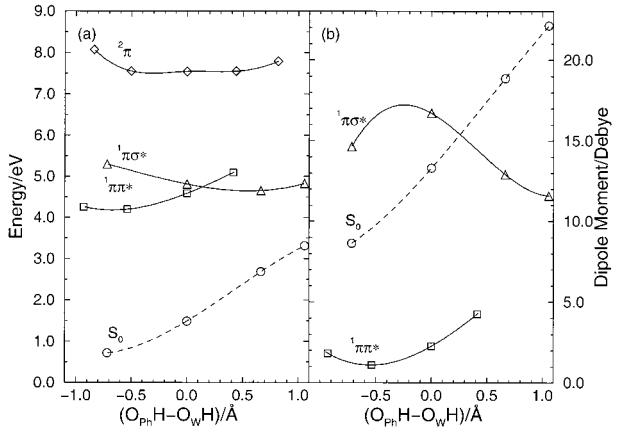

Figure 7. CASPT2 PE profiles (a) and CASSCF dipole moments (b) of the phenol$-(H_2O)_3$ complex in the electronic ground state (circles), the lowest $^1\pi\pi^*$ excited state (squares), the lowest $^1\pi\sigma^*$ state (triangles), and the $^2\pi$ ground state of the cation (diamonds) as a function of the hydrogen-transfer reaction coordinate.

The situation is different for the PW_3^+ cluster cation. Figure 7a shows that there exist two essentially isoenergetic minima of the $^2\pi$ PE function, representing non-PT and PT structures of Figure 6c,d, respectively. A Mulliken charge-distribution analysis indicates that the respective complexes are of the type $PhOH^+\cdots(H_2O)_3$ and $PhO\cdots H_3O^+(H_2O)_2$. The PT PE function of the cation is practically barrierless. These results are in agreement with previous UMP2 and DFT results.[20] It has also been inferred from various spectroscopic data that $n = 3$ is the critical size for PT in PhW_n^+ cluster cations.[4,9]

The dipole-moment functions of the relevant electronic states are presented in Figure 7b. As in the PhW_1 system, we observe a steep increase of the dipole moment of the S_0 state, reflecting a tendency for ion-pair formation when the proton is forced to move along the PT reaction path. The dipole-moment function of the $^1\pi\pi^*$ state shows less tendency for ion-pair formation. The dipole moment of the $^1\pi\sigma^*$ state saturates at a higher value with increasing $O_{Ph}H$ distance than for the PW_1 complex.

The ET process associated with the formation of the $^1\pi\sigma^*$ state is visualized in Figure 8. As found for the PhW_1 complex, the σ^* orbital is localized to a large extent near the solvent molecules already at the geometry of vertical excitation (Figure 8a). At the minimum geometry of the $^1\pi\sigma^*$ state (Figure 8b), the σ^* electron cloud has moved further away from the phenoxy radical. It is seen that the additional water molecules shield the electron from the H_3O^+ species in the center of the complex. This explains the higher dipole moment of hydrogen-transferred PhW_3 complex compared to PhW_1. The detachment of the σ^* electron from the aromatic radical and the formation of a water cage structure around the σ^* orbital (see Figure 8b) are very similar to the phenomena found previously in pyrrole$-$water and indole$-$water clusters.[39,40] The electron detachment from the chromophore is a unique property of the $^1\pi\sigma^*$ state: the π^* orbital of the $^1\pi\pi^*$ state is found to remain localized on the aromatic ring for all values of the $O_{Ph}H-O_WH$ distance.

D. Phenol$-NH_3$. The structure of the PhA_1 complex in the electronic ground state has been determined at the RHF level by Schiefke et al.[13] and Iwasaki et al.[41] and at the MP2 level by Sodupe et al.[19] and Re and Osamura.[20] The structure is of C_s symmetry, the ammonia nitrogen lying in the plane of phenol (Figure 9a). Some structural parameters obtained in the present MP2 optimization (not BSSE corrected) are indicated in Figure 9a. The hydrogen bond of PhA_1 is fairly strong, as reflected by a rather short NH bond length of 1.867 Å obtained at the MP2 level.

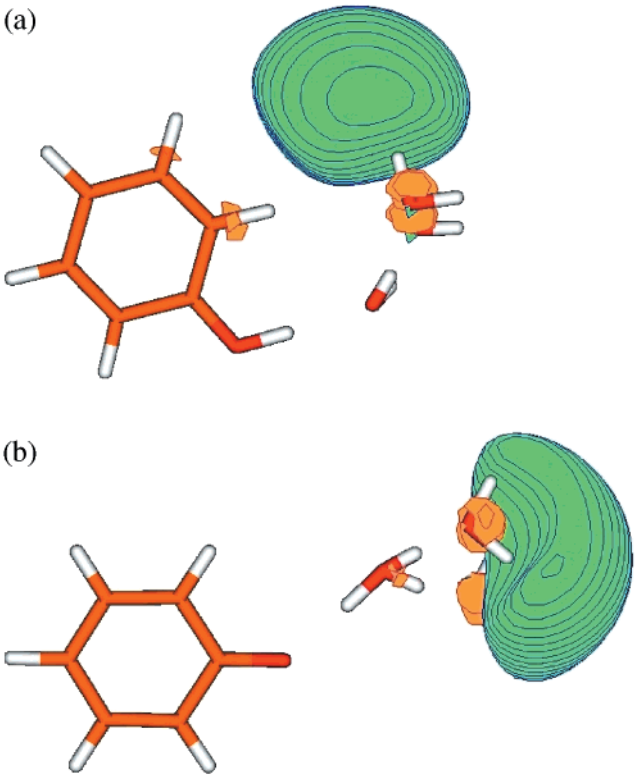

Figure 8. σ^* orbital obtained by a CASSCF calculation for the $^1\pi\sigma^*$ state of the phenol−$(H_2O)_3$ complex at the ground-state (a) and the $^1\pi\sigma^*$-state (b) equilibrium geometries.

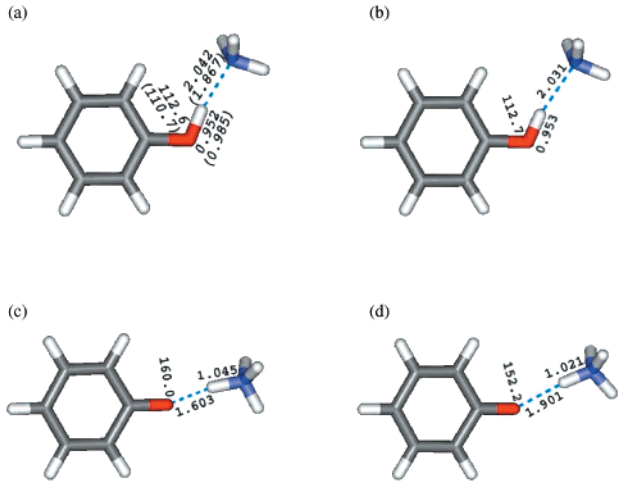

Figure 9. CASSCF equilibrium geometries of the phenol−ammonia complex in the S_0 state (a), the $^1\pi\pi^*$ excited state (b), the $^2\pi$ state of the cation (c), and the $^1\pi\sigma^*$ excited state (d). The S_0 geometry parameters optimized at the MP2 level are indicated in parentheses.

The structure of PhA_1 in the $S_1(\pi\pi^*)$ state has partially been optimized by Yi and Scheiner[15] at the CIS level. The $^1\pi\pi^*$ equilibrium structure optimized at the CASSCF level is displayed in Figure 9b. It is seen that the phenol−ammonia hydrogen bond in the $S_1(\pi\pi^*)$ state slightly contracts by 0.011 Å upon electronic excitation, as can be inferred from a comparison of the bond lengths in the respective states obtained at the same level of theory (CASSCF). This result is in accord with the conclusion of Yi and Scheiner[15] (based on RHF and CIS calculations) that the phenol−ammonia hydrogen bond is shortened upon excitation to the S_1 state.

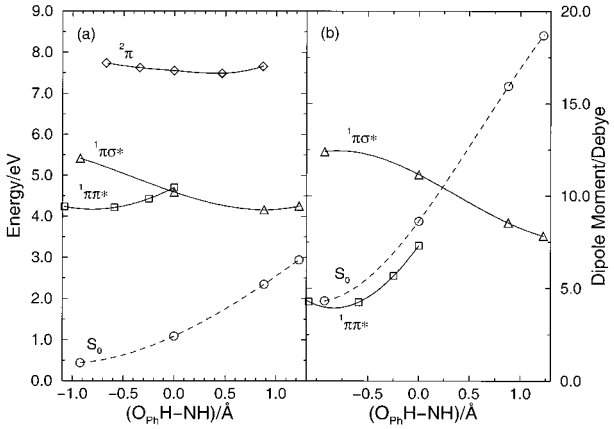

Figure 10. CASPT2 PE profiles (a) and CASSCF dipole moments (b) of the phenol−ammonia complex in the electronic ground state (circles), the lowest $^1\pi\pi^*$ excited state (squares), the lowest $^1\pi\sigma^*$ state (triangles), and the $^2\pi$ ground state of the cation (diamonds) as a function of the hydrogen-transfer reaction coordinate.

Structures of the PhA_1^+ complex have been determined at the UHF, UMP2, and DFT (B3LYP) levels.[15,19,20] At the UMP2 level both the non-PT structure $C_6H_5OH^+\cdots NH_3$ as well as the PT structure $C_6H_5O\cdots NH_4^+$ exist as stable minima, while geometry optimization at the DFT level yields only the PT structure.[19] The present CASSCF optimizations yield, like UMP2, both structures as local minima of the $^2\pi$ PE surface with the PT structure being lower in energy than the non-PT structure. CASPT2 single-point calculations predict the PT structure to be the only stable form of the PhA_1^+ complex. The CASSCF structure of the PT complex is shown in Figure 9c. The hydrogen bond between the phenoxy radical and NH_4^+ is very short (1.603 Å).

The CASSCF-optimized structure of the $^1\pi\sigma^*$ state is shown in Figure 9d. It is seen that the $^1\pi\sigma^*$ energy minimum corresponds to a phenoxy radical which is hydrogen bonded to a NH_4 radical. The OH bond length of 1.901 Å indicates that the $C_6H_5O\cdots NH_4$ hydrogen bond is stronger than the C_6H_5-$OH\cdots NH_3$ bond in both $^1\pi\pi^*$ and S_0 states. The $C_6H_5O\cdots NH_4$ complex is, however, more weakly bound than the corresponding $C_6H_5O\cdots H_3O$ complex (cf. Figure 3d).

The CASPT2 adiabatic excitation energies of the $^1\pi\pi^*$ and $^1\pi\sigma^*$ states are given in Table 1. As expected, the CASPT2 $^1\pi\pi^*$ excitation energy of PhA_1 (4.20 eV) is somewhat lower than the experimental[11] value (4.43 eV). While the $^1\pi\pi^*$ excitation energy of PhA_1 is not very different from the $^1\pi\pi^*$ excitation energies of the PhW clusters, the present calculations predict a significant lowering of the $^1\pi\sigma^*$ state at its optimized geometry. As shown by Table 1, the $^1\pi\sigma^*$ energy minimum is calculated to lie slightly below the $^1\pi\pi^*$ minimum for the PhA_1 cluster.

The CASPT2 PE profiles of the PhA_1 complex calculated along the reaction path for intracluster proton/hydrogen transfer are shown in Figure 10a. As for the PhW_n complexes discussed above, only the S_0 state, the lowest $^1\pi\pi^*$ and $^1\pi\sigma^*$ states and the ground state of the cation ($^2\pi$) are considered. The PE profiles of the S_0 state and the $^1\pi\pi^*$ state rise with increasing $O_{Ph}H$ distance, similar to the PhW_1 complex. Significant differences with respect to the PhW_1 system are found, on the other hand, for the $^1\pi\sigma^*$ and $^2\pi$ states. While the vertical excitation energy of the $^1\pi\sigma^*$ is essentially the same in PhW_1 and PhA_1 clusters, the $^1\pi\sigma^*$ energy is more strongly stabilized by hydrogen transfer in PhA_1. As a result, the crossing with

the $^1\pi\pi^*$ state occurs at lower energy, and the minimum of the $^1\pi\sigma^*$ surface lies below the minimum of the $^1\pi\pi^*$ surface (see Figure 10a). The excited-state hydrogen transfer process is predicted to be exothermic by 0.04 eV (0.9 kcal/mol) at the present level of theory. As explained above, it should be kept in mind that the $^1\pi\pi^*$ state is probably overstabilized relative to the $^1\pi\sigma^*$ state at the CASPT2 level, implying an underestimation of the exothermicity of the hydrogen-transfer process. As for the PhW_n complexes discussed above, the conical intersection of the $^1\pi\sigma^*$ state with the ground state occurring in bare phenol is removed in the PhA_1 complex.

In qualitative agreement with previous researchers,[15,19] we find a flat and barrierless PE function for PT in the cation. PT is thus predicted to occur readily in PhA_1^+, in contrast to the PhW_1^+ system (cf. Figure 4a).

The present results for PhA_1^+ are in full accord with a recent reinterpretation[42] of the experimental data[4−6] in terms of a barrierless PE function for PT in the PhA_1 cluster. The calculations confirm that proton transfer is an exothermic and activationless reaction in the PhA_1 cation. The existence of a substantial barrier preventing intracluster PT in PhA_1^+, which has previously been inferred from dissociative photoionization studies,[4,6] can be excluded on the basis of previous[15,19] and the present electronic-structure calculations.

The present results for the excited-state reaction-path PE profiles of PhA_1 correlate nicely with recent new experimental results and reinterpretations of previous experimental data for PhA_n clusters by Pino et al.,[7] Gregoire et al.,[43] and Ishiuchi et al.[44] These authors have argued that a "forgotten channel", namely hydrogen transfer rather than proton transfer, exists in the excited-state dynamics of small PhA_n clusters. Figure 10a shows that the hydrogen-transfer reaction is exoenergetic already for PhA_1 but is hindered by a barrier associated with the $^1\pi\pi^*-{}^1\pi\sigma^*$ curve crossing. This is consistent with the observation that hydrogen transfer is a slow process in PhA_1.[7,43] In analogy with the findings for PhW_n clusters discussed above, it is expected that the $^1\pi\sigma^*$ minimum is stabilized, relative to the $^1\pi\pi^*$ minimum, in larger PhA_n clusters, leading eventually to the disappearance of the barrier for the hydrogen-transfer reaction. Although calculations for larger PhA_n clusters still have to be performed, it can tentatively be concluded that the recent multiphoton ionization[7,43] and UV−IR double resonance[44] experiments have in fact detected the concerted proton−electron-transfer process associated with the transition from the $^1\pi\pi^*$ to the $^1\pi\sigma^*$ state in PhA_n complexes.

The dipole moments of the S_0, $^1\pi\pi^*$, and $^1\pi\sigma^*$ states as a function of the PT reaction coordinate are shown in Figure 10b. The increase of the S_0 and $^1\pi\pi^*$ dipole moments is an indication of the mixing of the covalent configuration with an ion-pair configuration. The existence of metastable ion-pair structures in the ground state as well as the $S_1(\pi\pi^*)$ excited states has previously been inferred from RHF and CIS calculations for PhA_5 clusters.[16,23] The polarity of $^1\pi\sigma^*$ state and the PE minimum is similar to that of the PhW_1 cluster.

The CASSCF σ^* orbital of the $^1\pi\sigma^*$ state of PhA_1 at the equilibrium geometries of the S_0 state and the $^1\pi\sigma^*$ state is shown in Figure 11. Similar as in PhW_1, the σ^* electron attaches to ammonia already in the vertically excited $^1\pi\sigma^*$ state (Figure 11a). Relaxation of the geometry results in the hydrogen-bonded complex of the phenoxy radical with the NH_4 radical. The characteristic Rydberg-type structure of the latter is clearly visible (Figure 11b). As in PhW clusters, the formation of the $^1\pi\sigma^*$ state involves a chromophore-to solvent charge-transfer process. The transfer of the electron provides the driving force for the detachment of the proton from phenol.

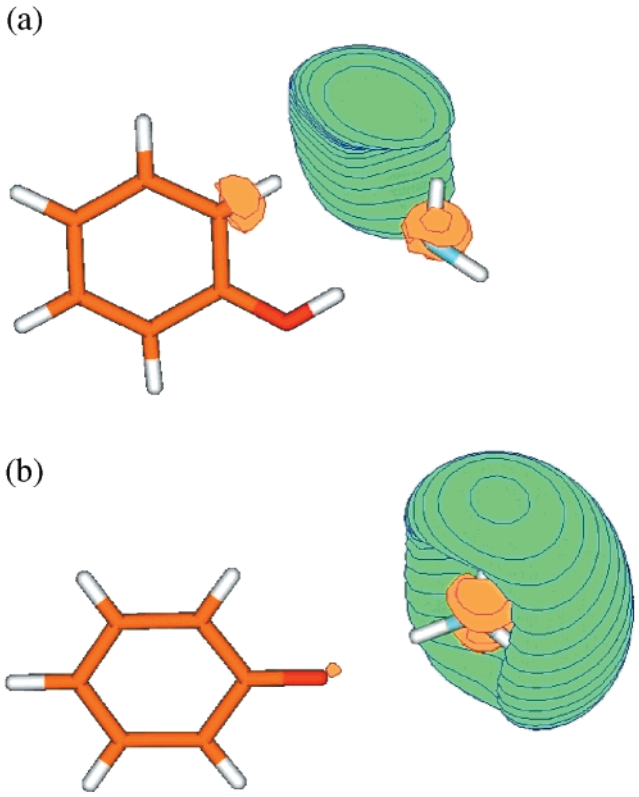

Figure 11. σ^* orbital obtained by a CASSCF calculation for the $^1\pi\sigma^*$ state of the phenol−ammonia complex at the ground-state (a) and at the $^1\pi\sigma^*$-state (b) minimum geometries.

4. Conclusions

Ab initio electronic-structure and reaction-path calculations have been performed to characterize the hydrogen detachment process in bare phenol and intracluster hydrogen-/proton-transfer processes in PhW and PhA clusters. It has been found that the lowest $^1\pi\sigma^*$ state plays a prominent role in the photochemistry of these systems. In bare phenol, the $^1\pi\sigma^*$ state predissociates the bound $S_1(\pi\pi^*)$ state, connecting the latter to a conical intersection with the S_0 state. An ultrafast internal-conversion channel thus opens above a certain excess energy in the S_1 state. Clustering of phenol with water or ammonia eliminates the $^1\pi\sigma^*-S_0$ conical intersection. In PhW and PhA complexes, the nonadiabatic transition to the $^1\pi\sigma^*$ state results in a configuration in which both an electron and a proton have been transferred from phenol to the solvent shell. This concerted electron−proton-transfer process in the excited-state manifold has been shown to be endothermic in PhW_1 and PhW_3 clusters but exothermic in the PhA_1 cluster. These computational results substantiate recent interpretations of multiphoton ionization and UV−IR double-resonance experiments in terms of an excited-state hydrogen-transfer process in PhA clusters.[7,43,44]

As a byproduct of the calculations, reaction-path PE profiles also have been obtained for PhW_1, PhW_3, and PhA_1 cluster cations. In agreement with conclusions derived from experimental data,[4,42] it is found that the critical size for PT in the cation is $n = 3$ for PhW clusters and $n = 1$ for PhA clusters.

The $^1\pi\sigma^*$ state is unique among the low-lying singlet states of PhW and PhA clusters insofar as spontaneous electron ejection from the chromophore to the solvent takes place. We have made this explicit by visualizations of the σ^* orbital for

representative cluster geometries. Electron ejection, i.e., the formation of hydrated electrons, is known to be an important channel in the UV photochemistry of tyrosine in aqueous solution.[45] The proton/electron transferred species identified by the present calculations can be considered as precursors of the hydrated electron produced by UV irradiation of phenol and tyrosine in liquid water.[45]

Acknowledgment. This work has been supported by the Deutsche Forschungsgemeinschaft and the Committee for Scientific Research of Poland (Grant No. 3 T09A 082 19).

References and Notes

(1) Creed, D. *Photochem. Photobiol*. **1984**, *39*, 537.
(2) Barry, B. A. *Photochem. Photobiol*. **1993**, *57*, 179.
(3) Zwier, T. S. *Annu. Rev. Phys. Chem*. **1966**, *47*, 205.
(4) Mikami, N. *Bull. Chem. Soc. Jpn.* **1995**, *68*, 683.
(5) Kleinermanns, K.; Gerhards, M.; Schmitt, M. *Ber. Bunsen-Ges. Phys. Chem*. **1997**, *101*, 1785.
(6) Syage, J. A. *Z. Phys. D* **1994**, *30*, 1.
(7) Pino, G.; Gregoire, G.; Dedonder-Lardeux, C.; Jouvet, C.; Martrenchard, S.; Solgadi, D. *Phys. Chem. Chem. Phys.* **2000**, *2*, 893.
(8) Schmitt, H.; Jacoby, Ch.; Gerhards, M.; Unterberg, C.; Roth, W.; Kleinermanns, K. *J. Chem. Phys*. **2000**, *113*, 2995.
(9) Kleinermanns, K.; Janzen, Ch.; Spangenberg, D.; Gerhards, M. *J. Phys. Chem. A* **1999**, *103*, 5232.
(10) Schütz, M.; Burgi, T.; Leutwyler, S.; Fischer, T. *J. Chem. Phys*. **1993**, *98*, 3763.
(11) Watabe, H.; Iwata, S. *J. Chem. Phys*. **1996**, *105*, 420.
(12) Gerhards, M.; Kleinermanns, K. *J. Chem. Phys*. **1995**, *103*, 7392.
(13) Schiefke, A.; Deusen, C.; Jacoby, C.; Gerhards, M.; Schmitt, M.; Kleinermanns, K. *J. Chem. Phys*. **1995**, *102*, 9197.
(14) Jacoby, C.; Roth, W.; Schmitt, M.; Janzen, C.; Spangenberg, D.; Kleinermanns, K. *J. Phys. Chem. A* **1998**, *102*, 4471.
(15) Yi, M.; Scheiner, S. *Chem. Phys. Lett*. **1996**, *262*, 567.
(16) Siebrand, W.; Zgierski, M. Z.; Smedarchina, Z. K.; Vener, M.; Kaneti, J. *Chem. Phys. Lett.* **1997**, *266*, 47.
(17) Janzen, Ch.; Spangenberg, D.; Roth, W.; Kleinermanns, K. *J. Chem. Phys*. **1999**, *110*, 9898.
(18) Hobza, P.; Burcl, R.; Spirko, V.; Dopfer, O.; Müller-Dethlefs, K.; Schlag, E. W. *J. Chem. Phys*. **1994**, *101*, 990.
(19) Sodupe, M.; Oliva, A.; Bertran, J. *J. Phys. Chem. A* **1997**, *101*, 9142.
(20) Re, S.; Osamura, Y. *J. Phys. Chem. A* **1998**, *102*, 3798.
(21) Siebrand, W.; Zgierski, M. Z.; Smedarchina, Z. K. *Chem. Phys. Lett*. **1997**, *279*, 377.
(22) Fang, W.-H. *J. Chem. Phys*. **2000**, *112*, 1204.
(23) Fang, W.-H.; Liu, R.-Z. *J. Chem. Phys*. **2000**, *113*, 5253.
(24) Sobolewski, A. L.; Domcke, W. *J. Phys. Chem. A* **1999**, *103*, 4494.
(25) Sobolewski, A. L.; Domcke, W. *Phys. Chem. Chem. Phys*. **1999**, *1*, 3065.
(26) Roos, B. O. *Adv. Quantum Chem*. **1987**, *69*, 399.
(27) Andersson, K.; Roos, B. O. In *Modern Electronic Structure Theory*; Yarkony, D. R., Ed.; World Scientific: Singapore, 1995; p 55.
(28) Gordon, M. S.; Binkley, J. S.; Pople, J. A.; Pietro, W. J.; Hehre, W. J. *J. Am. Chem. Soc*. **1982**, *104*, 2797.
(29) Schmidt, M. W.; et al. *J. Comput. Chem*. **1993**, *14*, 1347.
(30) Andersson, K.; et al. *MOLCAS, Version 4, User's Guide*; University of Lund: Lund, Sweden, 1997.
(31) van Mourik, T.; Price, S. L.; Clary, D. *Chem. Phys. Lett*. **2000**, *331*, 253.
(32) Krauss, M.; Jensen, J. O.; Hameka, H. F. *J. Phys. Chem*. **1994**, *98*, 9955.
(33) Gao, J.; Li, N.; Freindorf, M. *J. Am. Chem. Soc*. **1996**, *118*, 4912.
(34) Lorentzon, J.; Malmqvist, P.-A.; Fülscher, M.; Roos, B. O. *Theor. Chim. Acta* **1995**, *91*, 91.
(35) Berden, G.; Meerts, M. L.; Schmitt, M.; Kleinermanns, K. *J. Chem. Phys*. **1996**, *104*, 972.
(36) Stanley, R. J.; Castleman, A. W., Jr. *J. Chem. Phys*. **1991**, *94*, 7744.
(37) Watanabe, T.; Ebata, T.; Tanabe, S.; Mikami, N. *J. Chem. Phys*. **1996**, *105*, 408.
(38) Bürgi, T.; Schütz, M.; Leutwyler, S. *J. Chem. Phys*. **1995**, *103*, 6350.
(39) Sobolewski, A. L.; Domcke, W. *Chem. Phys. Lett*. **2000**, *321*, 479.
(40) Sobolewski, A. L.; Domcke, W. *Chem. Phys. Lett*. **2000**, *329*, 130.
(41) Iwasaki, A.; Fujii, A.; Watanabe, T.; Ebata, T.; Mikami, N. *J. Phys. Chem.* **1996**, *100*, 16053.
(42) Kim, H.-T.; Green, R. J.; Qian, J.; Anderson, S. L. *J. Chem. Phys*. **2000**, *112*, 5717.
(43) Gregoire, G.; Dedonder-Lardeux, C.; Jouvet, C.; Martrenchard, S.; Peremans, A.; Solgadi, D. *J. Phys. Chem. A* **2000**, *104*, 9087.
(44) Ishiuchi, S.; Saeki, M.; Sakai, M.; Fujii, M. *Chem. Phys. Lett*. **2000**, *322*, 27.
(45) Bent, D. V.; Hayon, E. *J. Am. Chem. Soc*. **1975**, *97*, 2599.